Nat Chem Biol. Author manuscript; available in PMC 2016 July 05.

Published in final edited form as:
Nat Chem Biol. ; 7(9): 617–623. doi:10.1038/nchembio.622.

Contributions of Counter-Charge in a Potassium Channel Voltage-Sensor Domain

Stephan A. Pless, **Jason D. Galpin**, **Ana P. Niciforovic**, and **Christopher A. Ahern***
Departments of Anesthesiology, Pharmacology and Therapeutics and Cellular and Physiological Sciences, University of British Columbia, 2350 Health Science Mall, Vancouver, BC, V6T 1Z3

Abstract

Voltage-sensor domains couple membrane potential to conformational changes in voltage-gated ion channels and phosphatases. Highly co-evolved acidic and aromatic side-chains assist the transfer of cationic side-chains across the transmembrane electric field during voltage-sensing. We investigated the functional contribution of negative electrostatic potentials from these residues to channel gating and voltage-sensing with unnatural amino acid mutagenesis, electrophysiology, voltage-clamp fluorometry and *ab initio* calculations. The data show that neutralization of two conserved acidic side-chains in transmembrane segments S2 and S3, Glu293 and Asp316 in *Shaker* potassium channels, have little functional effect on conductance-voltage relationships, although Glu293 appears to catalyze S4 movement. Our results suggest that neither Glu293 nor Asp316 engages in electrostatic state-dependent charge-charge interactions with S4, likely because they occupy, and possibly help create, a water-filled vestibule.

Introduction

Voltage-sensor domains endow ion and proton channels with the ability to control the passage of ions across cell membranes and can regulate phosphatase function in response to changes of transmembrane potential [1–3]. These domains contain four transmembrane alpha helical segments (S1–S4) and during voltage-sensing the actual voltage-sensor, the S4 segment, shuttles positively charged arginine and lysine side-chains across a highly focused electric field along a specialized trajectory: the negative resting potential of a quiescent cell keeps S4 in the resting or ‘down’ state, while membrane depolarization drives the positively charged S4 to the activated or ‘up’ state, a movement that is coupled from the voltage-sensor domain to the pore domain, ultimately leading to opening of the channel pore [4–9] C:\Users \pless\Documents\My Dropbox\PheGap2010\resubmission\Phe Gap abs intro and discussion.docx. The precise local environment of the S4 charges as they traverse the

*Correspondence: Dr. Christopher A. Ahern, cahern@interchange.ubc.ca, Tel: (604)-827-4393, Fax: (604)-822-6048.

Competing financial interests
The authors declare that they have no competing interests as defined by Nature Publishing Group, or other interests that might be perceived to influence the results and/or discussion reported in this paper.

Author Contributions
S.A.P. performed and analyzed the experiments, A.P.N. provided technical support and J.D.G. performed the chemical synthesis of all reagents. S.A.P and C.A.A designed the research and prepared the manuscript.

membrane is unknown, but the data available show that lipid [10–13] and proteinaceous [14–18] interactions are necessary for efficient voltage sensor function. In particular, three highly conserved acidic side-chains in S2 and S3, residues Glu283, Glu293 and Asp 316 in *Shaker* potassium channels, are proposed to interact functionally with S4 charges: while Glu283 resides near the extracellular end of S2, Glu293 and Asp316 are located near the cytosolic end of S2 and S3, respectively, and all three are proposed to form an electrostatic network with positively charged side-chains in S4 (Fig. 1a). Indeed, high-resolution structures [19,20] confirm the proximity of Glu293 and Asp316 to S4 residue Lys374 in the 'up' state of the voltage-sensor. The contribution of all three acidic residues to channel maturation and kinetics of folding are uncontested [21–23] and numerous studies have used conventional site-directed mutagenesis to demonstrate their importance for channel function [6,18,24–27], although their precise role has been difficult to pinpoint due to the lack of naturally occurring side-chain analogs that would allow one to investigate the specific contributions of charge and hydrogen bonding. To better address the chemical contributions of acidic side-chains close to S4 we turned to *in vivo* nonsense suppression [28] which allows for the site-directed incorporation of synthetic amino acids that possess subtle alterations of naturally occurring side-chains. This approach is especially useful in domains of the protein that are highly sensitive to side-chain replacements, such as S4 and its immediate surroundings. Importantly, the method also allows one to probe the electronegative surface potential of aromatic Phe, Tyr and Trp side-chains, which may also electrostatically assist S4 charge translocation. In particular, a highly conserved S2 phenylalanine residue, Phe290 in *Shaker* potassium channels, seems to be ideally placed to serve this purpose via a cation-pi interaction (Fig. 1a/b). Although experiments using unnatural derivatives of phenylalanine have suggested this interaction is absent in *Shaker* potassium channels, replacement with tryptophan at this position has striking effects on voltage-sensor function[20], raising the possibility of an induced intra-molecular cation-pi interaction with S4.

The data show that incorporation of the neutral synthetic glutamic acid derivative, nitrohomoalanine (**1**, Nha), at either position 293 or 316 in *Shaker* potassium channels had little functional impact on the conductance-voltage (GV) relationships. Voltage-clamp fluorometry of Glu293Nha channels showed this site appears to catalyze S4 movement, but neither of the acidic side-chains engages in electrostatic charge-charge interactions with S4, possibly because they promote the formation of water-filled vestibules, a notion supported by *ab initio* calculations. However, neutralization of Glu283 right-shifted the GV relationship with no change in slope factor, a result consistent with an open state stabilization through an electrostatic charge-charge interaction with S4. Surprisingly, the incorporation of a tryptophan residue at position 290 in S2 induced a strong cation-pi interaction with the S4 segment.

Results

Re-defining the Role of Acidic Residues in S2 and S3

A highly conserved Asp side-chain near the cytosolic end of S3 (Fig. 1b) has long been suggested to play a crucial role in channel function, as even the modest conventional Asn316 substitution in *Shaker* channels has a significant impact on the conductance-voltage

relationship (GV) and, to a greatly reduced extent, on the gating charge-voltage dependence (QV) [6,21]. While these effects could be explained through a disruption of an electrostatic charge-charge interaction with S4, it is also worthwhile to consider that Asn not only lacks the negative charge of Asp, but also replaces a hydrogen bond accepting oxygen with a hydrogen bond donating amino group. Consequently, the severity of the Asp to Asn mutation in position 316 (Fig. 2a) could be due to removal of charge and/or a secondary effect produced by the introduced hydrogen bond donor. More importantly, if an electrostatic charge-charge interaction between Asp316 and S4 charges is crucial for the stability of a particular channel conformation, then a considerable disruption of voltage dependence of conductance would be expected when the charged Asp side-chain is replaced with a neutral analog that displays no hydrogen bond donor capabilities. To directly test the effect of charge and hydrogen bonding at position 316, we aimed to replace the Asp carboxylate with an isosteric, uncharged nitro group but such an ideal replacement, nitroalanine, is not compatible with the *in vivo* nonsense suppression method, so we employed the neutral glutamic acid derivative nitrohomoalanine (Nha, Supplementary Results, Supplementary Fig. 1) [29]. Nha contains a neutral nitro group, which is a substantially weaker hydrogen bond acceptor than a carboxyl group: the energetics of nitro and carboxyl hydrogen bonding differ by ~ 2 kcal/mol [29,30]. Nha316 *Shaker* channels produced currents with virtually WT-like gating properties (Fig. 2a) with time constants for activation (τ ON) and deactivation (τ OFF) that showed no major differences compared to WT (Fig. 2b/c). This result suggests that a negative charge in position 316 is not required for normal channel function and suggests that Asp316 does not contribute to a particular state-dependent electrostatic charge-charge interaction with S4. However, a natural side-chain with strong hydrogen-bond donor capability (Asn), as well as an unnatural replacement with weak hydrogen-bond donor capability (**2**, Akp, Supplementary Fig. 2) had severe effects on channel function, potentially due to steric and/or electrostatic clashes with S4 charges resulting from the close proximity of two hydrogen bond donors.

Next, we investigated the role of a second highly conserved acidic side chain, Glu293 in S2 (Fig. 1b). Similar to Asp316 in S3, the relatively conservative conventional Gln293 substitution has been shown to cause severe effects on GV and QV [6,21]. Nha293 containing *Shaker* channels showed no significant differences in their GV relationships compared to WT channels (Fig. 2d), indicating that the negative charge is unlikely to stabilize a particular conformation of the channel. Reminiscent of the phenotypes observed at position 316, the more severe effects of the Gln substitution at position 293 observed by us (Fig. 2d) and others [6,21] are thus likely due to the strong hydrogen bond donor capabilities of the introduced Gln side-chain, possibly causing hydrogen bond clashes with S4 charges. However, because Nha293 led to substantially slowed time constants for both activation and deactivation (Fig. 2e/f), we sought to investigate if this effect was due to a change in kinetics of S4 movement itself or a change in coupling between the voltage-sensor domain and the pore domain. As conductance primarily reports on the state of the pore (i.e. open or closed), slower kinetics of the conductance could be due to two different scenarios: Glu293 directly interacts with S4 and neutralization of Glu293 directly slows down S4 movement (thus resulting in slower macroscopic current kinetics) or Glu293 does not interact with S4 but contributes to the coupling between the voltage-sensor domain and the pore domain and

neutralization of Glu293 disrupts efficient coupling between these two domains, thereby slowing opening and closing of the pore. To test if neutralization of Glu293 has a direct effect on S4 we sought to use an independent way to track S4 movement. The *in vivo* nonsense suppression method generally reduces expression levels, thus preventing classical gating current experiments, such as those performed on the non-conducting *Shaker* Trp434Phe background [31]. In contrast, performing voltage-clamp fluorometry (VCF) by labeling an introduced cysteine with an environmentally sensitive fluorophore tethered to the extracellular end of S4 can provide information on voltage-sensor movement at lower expression levels than those required for gating current measurements [32,33]. We performed VCF on Cys359 with tetramethylrhodamine-maleimide (TMRM) and Fig. 2g shows current and fluorescence traces recorded from channels with the single Cys359 mutation and from channels with both the Nha293 and the Cys359 substitutions. The results demonstrate that the voltage dependence of S4 movement is virtually unchanged by the Nha293 substitution (Fig. 2h), although we observed a significant slowing of both the ON and the OFF component of the fluorescence signal. As the Nha293 substitution not only slowed the activation and deactivation kinetics of the macroscopic current but also those of the fluorescence, we conclude that Nha293 has a direct effect on S4 movement. Taken together, these results indicate that a negative charge in position 293, although not essential for normal voltage-dependence, is a modest catalyst for S4 movement.

It is interesting that neutralization of either of the acidic side-chains in positions 293 and 316 had little functional consequence despite their putative proximity to Lys374 in the open conformation: a scant 2.9 and 3.2 angstroms from Glu293 or Asp316, respectively (Fig. 3a). Given their close proximity, it is possible that the neutralization of one side-chain is compensated by the other (still negatively charged) side-chain. To test this possibility, we created a channel containing TAG stop codons in both position 293 and 316 and although simultaneous incorporation of Nha resulted in a substantial reduction of current size, the GV was virtually unchanged compared to WT channels (Fig. 3b). Consistent with our findings from channels containing Nha at position 293 only, the simultaneous incorporation of Nha at positions 293 and 316 led to a significant slowing of the time constants for activation and deactivation of the macroscopic currents (Fig. 3c/d), confirming that a negative charge at position 293 is likely to catalyze S4 movement. These results demonstrate that single neutralizations are not functionally compensated by the remaining negative charge and argue against a particular state-dependent electrostatic charge-charge interaction between the basic side-chains in S4 and the acidic side-chains Glu293 and Asp316. In particular, these data do not support the possibility that these two acidic residues serve to stabilize the ‘up’ state of the channel via an electrostatic charge-charge interaction with the basic side-chain of Lys374, a finding that is further supported by our finding that neutralization of Lys374 by the isosteric neutral lysine analog 6-hydroxy norleucine (**3**, Hnl, Supplementary Fig. 1) had only minor effects on channel function (Supplementary Fig. 3).

How can the negative charges of Glu293 and Asp316 reside in such close proximity to the positive charge of Lys374 (and possibly other S4 charges) without participating in strong electrostatic charge-charge interactions, as demonstrated by the data obtained from neutral unnatural analogs? It is possible that these acidic side-chains reside in, and/or contribute to

the formation of a hydrophilic water-filled vestibule [10,34–38], which in turn creates an energetically favorable environment for the charged S4 segment. Interestingly, the strength of electrostatic interactions between oppositely charged moieties is highly dependent on the dielectric of the environment, with aqueous environments dramatically weakening such potential interactions [39]. To test if this prediction is true for the specific geometries of the Glu293/Lys374 and Asp316/Lys374 pairs, we conducted *ab initio* calculations with geometrically constrained side-chain pairs based on available crystallographic data [19] and found that high dielectric constants, such as present in aqueous environments, significantly weaken potential electrostatic charge-charge interactions (Fig. 3e).

The Role of an Extracellular Acidic Side-Chain in S2

Next, we investigated the contributions of a highly conserved acidic side chain, Glu283 in *Shaker*, that has been suggested to play a critical role in channel function [16,18,21,27]. Structural data show the close proximity of Glu283 to Arg368 and Arg371 in the 'up' state of S4 (Fig. 4a) [19], raising the possibility of an electrostatic charge-charge interaction crucial for the channel open state. Consistent with the charge of Glu283 playing a role in open state stabilization, the neutral Gln283 substitution lead to a dramatic right-shift in the GV (Fig. 4b). However, given the results from Glu293 and Asp316, a secondary effect mediated by the Gln amide could not be excluded. To directly test the effect of charge removal, Nha was incorporated at position 283 and we observed a 20 mV right-shift in the GV (Fig. 4b). Additionally, the time constants for activation remained unchanged (Fig. 4c), while the time constants for deactivation were significantly faster (Fig. 4d). Taken together, these results demonstrate that the negative charge at Glu283 is likely to contribute to an electrostatic charge-charge interaction that stabilizes the channel open state. However, it is interesting to note that the electrostatic contribution was less than one would predict from the dramatic phenotype induced by conventional mutagenesis: the right-shift in the GV was only around 20 mV for Nha283, whereas it was roughly 70 mV for Gln283.

Aromatic Contributions at Position 290 in S2

In theory, an aromatic side-chain could catalyze the transmembrane passage of S4 charges through an electrostatic cation-pi interaction and a highly conserved Phe in S2 had been suggested to assist S4 movement via this mechanism based on structural data [19]. However, although this residue is present and likely very close to S4 charges in most voltage gated potassium, sodium and calcium channels, such an interaction has recently been shown to be absent in *Shaker* channels by using unnatural amino acids, including fluorinated phenylalanine derivatives, 4-F-Phe (**4**), 3,5-F_2-Phe (**5**) and 3,4,5-F_3-Phe (**6**) [20] (see also Supplementary Fig. 4). Intriguingly, a recent study has shown that the Trp290 substitution leads to a pronounced stabilization of the channel open state [20]. We thus investigated the possibility that introducing Trp at position 290 (Fig. 5a) could form an induced cation-pi interaction by expressing *Shaker* potassium channels with a series of fluorinated Trp derivatives at position 290: 5-F-Trp (**7**), 5,7-F_2-Trp (**8**), 5,6,7-F_3-Trp (**9**) and 4,5,6,7-F_4-Trp (**10**) (see also Supplementary Fig. 1). Each added fluorine atom produced a stepwise right-shift in the GV (Fig. 5b and Supplementary Table 1), showing that the electronegative surface potential of Trp contributes to a cation-pi interaction, likely with Lys374. If this hypothesis is correct, then replacing Lys with Arg in position 374 should reduce the effect

observed by fluorination, as the more focused primary amine of Lys is predicted to form cation-pi interactions that are 1.5 to 3.5-fold stronger than those formed by Arg [40]. Indeed, we found that fluorination on the Arg374 background also leads to stepwise right-shift in the GV (Fig. 5c), but the effect of fluorination was reduced almost 2.5-fold (Supplementary Table 1). The plot in Fig. 5d formalizes the cation-pi interaction at Trp290 (with either Lys or Arg in position 374) through the linear relationship between the experimentally determined $ZFV_{½}$ values 41 and the calculated cation-pi binding ability of the fluorinated Trp derivatives [42]. Although we cannot exclude the possibility that other S4 charges may also contribute to the cation-pi interaction at Trp290, our results suggest that the dominating interaction is formed between Lys374 and Trp290, an idea that is consistent with crystallographic data (Fig. 5a) [20] as well as the apparent open state stabilization induced by Trp290 that is dependent on a lysine in position 374 (as reflected by the potent left-shifts in the GV and the QV of these channels [20]).

Discussion

How are the positive charges of S4 stabilized in the hydrophobic core of the membrane? This question has long held considerable attention, with negatively charged side-chains in the S2 and S3 segments proposed to play a major role in possible mechanisms [14,16]. The side chains Glu293 and Asp316 in *Shaker* potassium channels are located near the cytosolic end of S4 and have been proposed form electrostatic charge-charge interactions with S4 [6,19–21,24–27]. Results with an unnatural neutral analog of Glu demonstrate that a negative charge is not required for the stability of a particular channel state. We feel the data are in agreement with the multitude of previous experiments that have highlighted the importance of these side-chains. In fact, neutralizations of Glu293 alone or simultaneous neutralization of Lys374 with Glu293 or Asp316 have earlier been shown to be functional and, importantly, to cause a left-shifted conductance-voltage relations, while neutralization of Asp316 have been shown to cause a right-shift in the conductance-voltage relation, both results that do not support the idea that the negative charges of Glu293 or Asp316 stabilize a particular (and likely identical) channel state [6,21]. In theory, however, it is possible that the acidic side-chains Glu293 and Asp316 form electrostatic interactions with basic S4 residues in all S4 conformations, thereby leaving the conductance-voltage relation unchanged. We believe this scenario is unlikely for three reasons: firstly, lowering the energy barrier between S4 conformations (by removing the negative charges at positions 293 and 316) should accelerate channel gating, which stands in contrast to our observation that Nha293 (but not Nha316) slowed down gating. Consequently, both our finding that Nha316 did not significantly affect the kinetics of gating and Nha293 slowed them down argues against this notion. Secondly, it seems unlikely that arginines (Arg362, Arg365, Arg368, Arg371) and lysines (Lys374), with their vastly different stereochemistry and charge-distribution, would interact precisely with the same energy with Glu293 and Asp316, a point made empirically by our data showing different cation-pi interaction energies at Trp290 for Lys374 or Arg374. Finally, it should be noted that a recent computational study has suggested that Asp316 points away from Lys374, making direct electrostatic interactions between Asp316 and S4 charges unlikely [35]. Taken together, these observations argue against the possibility that Glu293 and Asp316 interact electrostatically via charge-charge interactions with S4 in all

conformations. Instead, we suggest that the side-chains of Asp316 and Glu293, along with the hydration needs of S4 charges, occupy and promote the formation of water filled vestibules in the voltage-sensor domain. The high local dielectric associated with an aqueous environment serves to reduce the interaction energy between charged side-chains, and consequently can prevent electrostatic charge-charge interactions, a phenomenon shown previously [39] and confirmed here using *ab initio* calculations. In fact, there is a large body of evidence that points to the existence of a well-hydrated S4 segment; the accessibility of substituted cysteine residues along the S4 segment [7], introduced histidine residues that can create proton-selective transporters and channels [36,37], results from electron paramagnetic resonance (EPR) studies [34,38], the existence of so-called 'omega' currents through the voltage-sensor [43,44] and the observation that isolated voltage-sensor domains spontaneously form such crevices by distorting the bilayer [10]. And while the presence of aqueous vestibules were difficult to reconcile with early crystal structures of voltage-gated potassium channels [45], recent structures show that the S4 segment could readily accommodate such architecture [19,46]. Interestingly, the loss of charge at Glu293 results in a significant slowing of S4 movement as well as a slowing of channel activation and deactivation kinetics. If, indeed, Glu293 contributes to the focusing of the transmembrane electric field by supporting the formation of water filled vestibules, neutralization at this site may result in the expansion or 'de-focusing' of the transmembrane electric field due to the decrease in the local dielectric. The prediction of such an expansion of the transmembrane electric field around S4 would be an increased energy barrier for the movement of the charged S4 segment, resulting in a pronounced slowing of S4 movement. As shown in Fig. 2 this is, in fact, what we observe experimentally.

The results also provide an explanation for why negative charge is highly conserved in positions 293 and 316, as Glu and Asp are the only naturally occurring side-chains that contain a hydrophilic head group without a propensity for donating hydrogens which could result in steric and/or electrostatic clashes with S4 charges under physiological conditions. We suggest that either of two (or both) types of disruptive interactions could occur between Asn or Gln side-chains and S4 charges. This possibility would explain why Asn316 and Gln293 have such profound effects on channel function yet the Nha side-chain, with its neutral nitro moiety devoid of hydrogens, produces normal channels with wild-type like function (Fig. 2d). Lastly, it should be noted that the incorporation efficiency of unnatural amino acids using nonsense suppression is highly variable from site to site within the same protein and our results consequently do not inform on channel maturation or voltage-sensor domain folding kinetics, two aspects that may be affected by mutations to the acidic side chains tested here [21–23,47].

If the high local dielectric prevents Lys374 from forming a strong electrostatic charge-charge interaction with Glu293 or Asp316, how can this same side-chain form a (predominantly electrostatic) cation-pi interaction with an introduced Trp at position 290? The answer lies in the inherent solvent-dependence of the two interactions: while electrostatic charge-charge interactions between two oppositely charged moieties are highly susceptible to the local dielectric, cation-pi interactions are not [39]. In fact, in an aqueous environment cation-pi interactions are more stable than electrostatic interactions between two oppositely charged moieties, providing a possible explanation for the observed strong interaction between

Lys374 and Trp290 but not between Lys374 and either Glu293 or Asp316. Based on crystallographic data and theoretical predictions, cation-pi interactions have previously proposed to play a role in structural contexts [19,40] yet direct, functional evidence for them has thus far been missing. Therefore the empirical characterization of the interaction between Lys374 and Trp290 here serves as a proof-of-principle observation for intra-molecular cation-pi interactions in the structural context. Although the data could be interpreted to confirm the close proximity of Lys374 to Trp290 in the open state *in vivo*, suggesting that the conformation captured in recent crystallographic structures [19,20] likely represents a true open state, it is crucial to consider that S4 can enter a 'relaxed' state in the presence of an open pore [48,49]. Regardless, the observation of a cation-pi interaction between Lys374 and Trp290 is mechanistically insightful given the strong geometric preference of cation-pi interaction, *en-face* vs. on edge, suggesting that S4 charges, and in particular Lys374, come within a few angstroms from the face of the introduced tryptophan side-chain, providing further constraints on the 'up' state of S4 *in vivo*. The strict geometric requirements of cation-pi interactions are also likely the reason for the observed preference for Trp over Phe at position 290: while both side-chains are aromatic, the indole ring of Trp displays substantially different properties with respect to geometry and distance to the α carbon when compared to Phe. It should be noted that if the other charges in the S4 segment were to share a common pathway through the electric field, it would bring them in close proximity to the aromatic side-chain in position 290, leading to the possibility that the introduced Trp side-chain consummates multiple cation-pi interactions with S4. Taken together, the results shed new light on the contributions of highly conserved acidic and aromatic side chains in voltage-sensor domains.

Methods

Molecular Biology and *in vivo* nonsense suppression

The channel used was *Shaker* H4 with deletion of residues 6–46 to remove N-type inactivation and the point mutations C301S, C308S and T449V/F unless otherwise stated (in pBSTA). Successful incorporation of mutations was confirmed by automated sequencing. Complementary RNA was transcribed from the cDNA using the mMessage mMachine kit (Ambion, Austin, TX). Stage V–VI *Xenopus* oocytes were prepared as previously described [50], and injected with cRNA alone or cRNA plus tRNA (see below). After injection, oocytes were incubated for 12 to 48 h at 18°C. The principle of the *in vivo* nonsense suppression methodology was described previously [28]. The synthesis of the unnatural amino acids 2-amino-4-ketopentanoic acid (Akp) and nitrohomoalanine (Nha) was performed as previously described [29]. The synthesis of 6-hydroxy norleucine (Hnl) is described in Supplementary Methods. The fluorinated phenylalanine and tryptophan derivatives were purchased from Asis Chem (Watertown, MA) or Sigma Aldrich (St. Louis, MO). Unnatural amino acids (aa) were protected with nitroveratryloxycarbonyl (NVOC) and activated as the cyanomethyl ester, which was then coupled to the dinucleotide pdCpA (Dharmacon, CO, USA). This aminoacyl dinucleotide was subsequently ligated to a modified (G73) *Tetrahymena thermophila* tRNA. The aminoacylated tRNA-aa was deprotected by UV irradiation immediately before co-injection with the cRNA for the channel. In a typical experiment, 80 ng of tRNA-aa and 25 ng of channel cRNA were injected in a 50 nL volume. In control

experiments, the cRNA alone or the cRNA together with a tRNA coupled to pdCpA but without an appended aa were injected. Currents for Phe290TAG, Glu283TAG, Glu293TAG, Asp316TAG or Lys374TAG constructs were never larger than those recorded from oocytes injected with water, even at very large depolarizations (< 500 nA at + 100mV for 100 ms, n = 5 each).

Two Electrode Voltage-Clamp and Voltage-Clamp Fluorometry (VCF)

Voltage-clamped potassium and sodium currents were recorded with two microelectrodes using an OC-725C voltage clamp (Warner, Hamden, CT) in a standard Ringers solution (in mM): 116 NaCl, 2 KCl, 1 $MgCl_2$, 0.5 $CaCl_2$, 5 HEPES (pH 7.4). All recordings were performed at 20–22°C. Glass microelectrodes had resistances of 0.1 – 1 MΩ and were backfilled with 3M KCl. The holding potential was −80 mV and −100 mV for experiments with potassium channels and sodium channels, respectively. Depolarizing voltage-pulses were given for 20 – 100 ms (conventional two-electrode voltage-clamp) or 150 ms (for VCF experiments). 5 and 10 mV increments for conventional two-electrode voltage-clamp and VCF, respectively. For VCF, oocytes were labeled for 20 min. with 10 μM tetramethylrhodamine-5-maleimide (TMRM; Invitrogen, Carlsbad, CA) on ice in a depolarizing solution containing (in mM) 100 KCl, 1.5 $MgCl_2$, 0.5 $CaCl_2$, and 10 HEPES (pH 7.4) and subsequently washed and stored in Ringers solution. Fluorometry was simultaneously performed with two electrode voltage-clamp on an Olympus IX51 inverted microscope and a PMT400 photomultiplier tube (IonOptix, Milton, MA). A X-Cite 120 Q (Lumen Dynamics Group, Mississauga, ON, Canada) served as a light source, a Lambda SC as a shutter (Sutter Instruments, Novato, CA). The sampling frequency for the fluorescence signal was 1 kHz and analyzed traces were an average of 20–50 sweeps; displayed signal traces were offline filtered at 300–800 Hz. Conductance-voltage (GV) relationships were derived by plotting the isochronal tail current amplitudes (the current amplitude measured after stepping from the test potential back to a holding potential of 80 mV) as a function of the depolarizing pulse potential. Similarly, for fluorescence-voltage (FV) relationships, the peak fluorescence signals (FV) was plotted against the depolarizing pulse potential. All displayed current and fluorescence traces show the full active voltage range of GVs and FVs, respectively. All data = mean ± S.E.M.

Supplementary Material

Refer to Web version on PubMed Central for supplementary material.

Acknowledgments

We thank Dr. Richard Horn, Dr. Harley Kurata and Dr. Sam Goodchild for helpful discussions. This work was supported by the Canadian Institutes of Health Research (56858), the Heart and Stroke Foundation of Canada, the Michael Smith Foundation for Health Research (to C.A.A.) and a postdoctoral fellowship by the Heart and Stroke Foundation of Canada (to S.A.P.).

Abbreviations

Akp	2-amino-4-ketopentanoic acid
Arg	arginine

Asn	asparagine
Asp	aspartic acid
Cys	cysteine
ESP	electrostatic surface potential
FV	fluorescence-voltage relation
Gln	glutamine
Glu	glutamic acid
GV	conductance-voltage relation
K_V1.2/K_V2.1	voltage-gated potassium channel isoforms 1.2 and 2.1, respectively
Lys	lysine
Nha	nitrohomoalanine
Phe	phenylalanine
QV	gating charge-voltage dependence
TMRM	tetramethylrhodamine-maleimide
Trp	tryptophane
S1–S6	transmembrane segments 1 to 6
VCF	voltage-clamp fluorometry (VCF)
WT	wild type

References

1. Hille, B. Ion channels of excitable membranes. 3. Sinauer; 2001.
2. Murata Y, Iwasaki H, Sasaki M, Inaba K, Okamura Y. Phosphoinositide phosphatase activity coupled to an intrinsic voltage sensor. Nature. 2005; 435:1239–1243. [PubMed: 15902207]
3. Ramsey IS, Moran MM, Chong JA, Clapham DE. A voltage-gated proton-selective channel lacking the pore domain. Nature. 2006; 440:1213–1216. [PubMed: 16554753]
4. Ahern CA, Horn R. Focused electric field across the voltage sensor of potassium channels. Neuron. 2005; 48:25–29. [PubMed: 16202706]
5. Aggarwal SK, MacKinnon R. Contribution of the S4 segment to gating charge in the Shaker K+ channel. Neuron. 1996; 16:1169–1177. [PubMed: 8663993]
6. Seoh SA, Sigg D, Papazian DM, Bezanilla F. Voltage-sensing residues in the S2 and S4 segments of the Shaker K+ channel. Neuron. 1996; 16:1159–1167. [PubMed: 8663992]
7. Yang N, George AL Jr, Horn R. Molecular basis of charge movement in voltage-gated sodium channels.
8. Ahern CA, Horn R. Specificity of charge-carrying residues in the voltage sensor of potassium channels. J Gen Physiol. 2004; 123:205–216. [PubMed: 14769847]

9. Chanda B, Bezanilla F. A common pathway for charge transport through voltage-sensing domains. Neuron. 2008; 57:345–351. [PubMed: 18255028]
10. Krepkiy D, et al. Structure and hydration of membranes embedded with voltage-sensing domains. Nature. 2009; 462:473–479. [PubMed: 19940918]
11. Milescu M, et al. Interactions between lipids and voltage sensor paddles detected with tarantula toxins. Nat Struct Mol Biol. 2009; 16:1080–1085. [PubMed: 19783984]
12. Schmidt D, Jiang QX, MacKinnon R. Phospholipids and the origin of cationic gating charges in voltage sensors. Nature. 2006; 444:775–779. [PubMed: 17136096]
13. Xu Y, Ramu Y, Lu Z. Removal of phospho-head groups of membrane lipids immobilizes voltage sensors of K+ channels. Nature. 2008; 451:826–829. [PubMed: 18273018]
14. Armstrong CM. Sodium channels and gating currents. Physiol Rev. 1981; 61:644–683. [PubMed: 6265962]
15. Bosmans F, Martin-Eauclaire MF, Swartz KJ. Deconstructing voltage sensor function and pharmacology in sodium channels. Nature. 2008; 456:202–208. [PubMed: 19005548]
16. Catterall WA. Ion channel voltage sensors: structure, function, and pathophysiology. Neuron. 2010; 67:915–928. [PubMed: 20869590]
17. Li-Smerin Y, Hackos DH, Swartz KJ. alpha-helical structural elements within the voltage-sensing domains of a K(+) channel. J Gen Physiol. 2000; 115:33–50. [PubMed: 10613917]
18. Wu D, et al. State-dependent electrostatic interactions of S4 arginines with E1 in S2 during Kv7.1 activation. J Gen Physiol. 2010; 135:595–606. [PubMed: 20479111]
19. Long SB, Tao X, Campbell EB, MacKinnon R. Atomic structure of a voltage-dependent K+ channel in a lipid membrane-like environment. Nature. 2007; 450:376–382. [PubMed: 18004376]
20. Tao X, Lee A, Limapichat W, Dougherty DA, MacKinnon R. A gating charge transfer center in voltage sensors. Science. 2010; 328:67–73. [PubMed: 20360102]
21. Papazian DM, et al. Electrostatic interactions of S4 voltage sensor in Shaker K+ channel. Neuron. 1995; 14:1293–1301. [PubMed: 7605638]
22. Tiwari-Woodruff SK, Schulteis CT, Mock AF, Papazian DM. Electrostatic interactions between transmembrane segments mediate folding of Shaker K+ channel subunits. Biophys J. 1997; 72:1489–1500. [PubMed: 9083655]
23. Zhang L, et al. Contribution of hydrophobic and electrostatic interactions to the membrane integration of the Shaker K+ channel voltage sensor domain. Proc Natl Acad Sci U S A. 2007; 104:8263–8268. [PubMed: 17488813]
24. Planells-Cases R, Ferrer-Montiel AV, Patten CD, Montal M. Mutation of conserved negatively charged residues in the S2 and S3 transmembrane segments of a mammalian K+ channel selectively modulates channel gating. Proc Natl Acad Sci U S A. 1995; 92:9422–9426. [PubMed: 7568145]
25. DeCaen PG, Yarov-Yarovoy V, Sharp EM, Scheuer T, Catterall WA. Sequential formation of ion pairs during activation of a sodium channel voltage sensor. Proc Natl Acad Sci U S A. 2009; 106:22498–22503. [PubMed: 20007787]
26. DeCaen PG, Yarov-Yarovoy V, Zhao Y, Scheuer T, Catterall WA. Disulfide locking a sodium channel voltage sensor reveals ion pair formation during activation. Proc Natl Acad Sci U S A. 2008; 105:15142–15147. [PubMed: 18809926]
27. Silverman WR, Roux B, Papazian DM. Structural basis of two-stage voltage-dependent activation in K+ channels. Proc Natl Acad Sci U S A. 2003; 100:2935–2940. [PubMed: 12606713]
28. Nowak MW, et al. In vivo incorporation of unnatural amino acids into ion channels in Xenopus oocyte expression system. Methods Enzymol. 1998; 293:504–529. [PubMed: 9711626]
29. Cashin AL, Torrice MM, McMenimen KA, Lester HA, Dougherty DA. Chemical-scale studies on the role of a conserved aspartate in preorganizing the agonist binding site of the nicotinic acetylcholine receptor. Biochemistry. 2007; 46:630–639. [PubMed: 17223685]
30. Kelly TR, Kim MH. Relative binding affinity of carboxylate and its isosteres: Nitro, phosphate, phosphonate, sulfonate and σ-lactone. J Am Chem Soc. 1994; 116:7072–7080.

31. Perozo E, MacKinnon R, Bezanilla F, Stefani E. Gating currents from a nonconducting mutant reveal open-closed conformations in Shaker K+ channels. Neuron. 1993; 11:353–358. [PubMed: 8352943]
32. Cha A, Bezanilla F. Characterizing voltage-dependent conformational changes in the Shaker K+ channel with fluorescence. Neuron. 1997; 19:1127–1140. [PubMed: 9390525]
33. Mannuzzu LM, Moronne MM, Isacoff EY. Direct physical measure of conformational rearrangement underlying potassium channel gating. Science. 1996; 271:213–216. [PubMed: 8539623]
34. Chakrapani S, Cuello LG, Cortes DM, Perozo E. Structural dynamics of an isolated voltage-sensor domain in a lipid bilayer. Structure. 2008; 16:398–409. [PubMed: 18334215]
35. Chen X, Wang Q, Ni F, Ma J. Structure of the full-length Shaker potassium channel Kv1.2 by normal-mode-based X-ray crystallographic refinement. Proc Natl Acad Sci U S A. 2010; 107:11352–11357. [PubMed: 20534430]
36. Starace DM, Bezanilla F. Histidine scanning mutagenesis of basic residues of the S4 segment of the shaker k+ channel. J Gen Physiol. 2001; 117:469–490. [PubMed: 11331357]
37. Starace DM, Bezanilla F. A proton pore in a potassium channel voltage sensor reveals a focused electric field. Nature. 2004; 427:548–553. [PubMed: 14765197]
38. Chakrapani S, Sompornpisut P, Intharathep P, Roux B, Perozo E. The activated state of a sodium channel voltage sensor in a membrane environment. Proc Natl Acad Sci U S A. 2010; 107:5435–5440. [PubMed: 20207950]
39. Gallivan JP, Dougherty DA. A Computational Study of Cation-π Interactions vs Salt Bridges in Aqueous Media: Implications for Protein Engineering. J Am Chem Soc. 2000; 122:870–874.
40. Gallivan JP, Dougherty DA. Cation-pi interactions in structural biology. Proc Natl Acad Sci U S A. 1999; 96:9459–9464. [PubMed: 10449714]
41. Yifrach O, MacKinnon R. Energetics of pore opening in a voltage-gated K(+) channel. Cell. 2002; 111:231–239. [PubMed: 12408867]
42. Zhong W, et al. From ab initio quantum mechanics to molecular neurobiology: a cation-pi binding site in the nicotinic receptor. Proc Natl Acad Sci U S A. 1998; 95:12088–12093. [PubMed: 9770444]
43. Sokolov S, Scheuer T, Catterall WA. Gating pore current in an inherited ion channelopathy. Nature. 2007; 446:76–78. [PubMed: 17330043]
44. Tombola F, Pathak MM, Gorostiza P, Isacoff EY. The twisted ion-permeation pathway of a resting voltage-sensing domain. Nature. 2007; 445:546–549. [PubMed: 17187057]
45. Jiang Y, et al. X-ray structure of a voltage-dependent K+ channel. Nature. 2003; 423:33–41. [PubMed: 12721618]
46. Jogini V, Roux B. Dynamics of the Kv1.2 voltage-gated K+ channel in a membrane environment. Biophys J. 2007; 93:3070–3082. [PubMed: 17704179]
47. Sato Y, Sakaguchi M, Goshima S, Nakamura T, Uozumi N. Integration of Shaker-type K+ channel, KAT1, into the endoplasmic reticulum membrane: synergistic insertion of voltage-sensing segments, S3–S4, and independent insertion of pore-forming segments, S5-P-S6. Proc Natl Acad Sci U S A. 2002; 99:60–65. [PubMed: 11756658]
48. Lacroix JJ, Labro AJ, Bezanilla F. Properties of deactivation gating currents in shaker channels. Biophys J. 2011; 100:L28–30. [PubMed: 21354387]
49. Villalba-Galea CA, Sandtner W, Starace DM, Bezanilla F. S4-based voltage sensors have three major conformations. Proc Natl Acad Sci U S A. 2008; 105:17600–17607. [PubMed: 18818307]
50. Pless SA, et al. A cation-pi interaction in the binding site of the glycine receptor is mediated by a phenylalanine residue. J Neurosci. 2008; 28:10937–10942. [PubMed: 18945901]

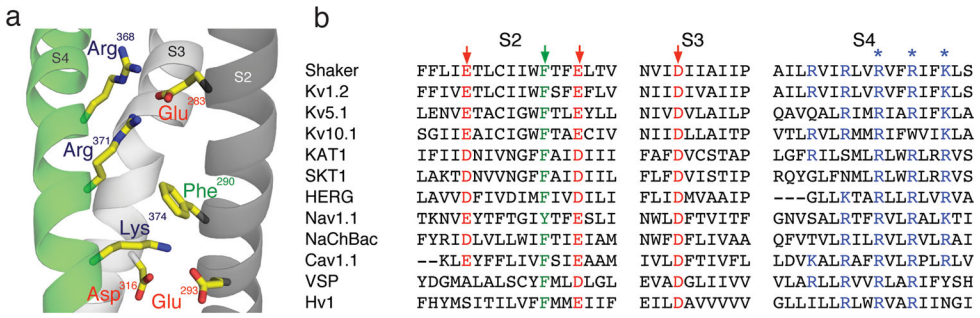

Figure 1. Model of transmembrane segments 2–4 and sequence alignment

(a) Model showing transmembrane segments 2 (dark grey), 3 (light grey) and 4 (green), highlighted are Glu283, Glu293, Asp316, Arg 368, Arg371 and Lys374 (PDB 2R9R); (b) Sequence alignment of various voltage-dependent membrane proteins: *Shaker* (GI: 13432103), Kv1.2 (GI:52000923), Kv5.1 (GI: 20070166), Kv10.1 (GI: 22164088), KAT1 (GI:15237407), SKT1 (GI:1514649), HERG (GI:4557729), Nav1.1 (115583677), Cav1.1 (GI:110349767), NaChBac (GI:10174118), VSP (GI:76253898), Hv1 (GI:91992155). Conserved residues are color-coded: acidic = red, basic = blue and aromatic = green. The arrows indicate residues studied here, the asterisks indicate Arg368, Arg371 and Lys374.

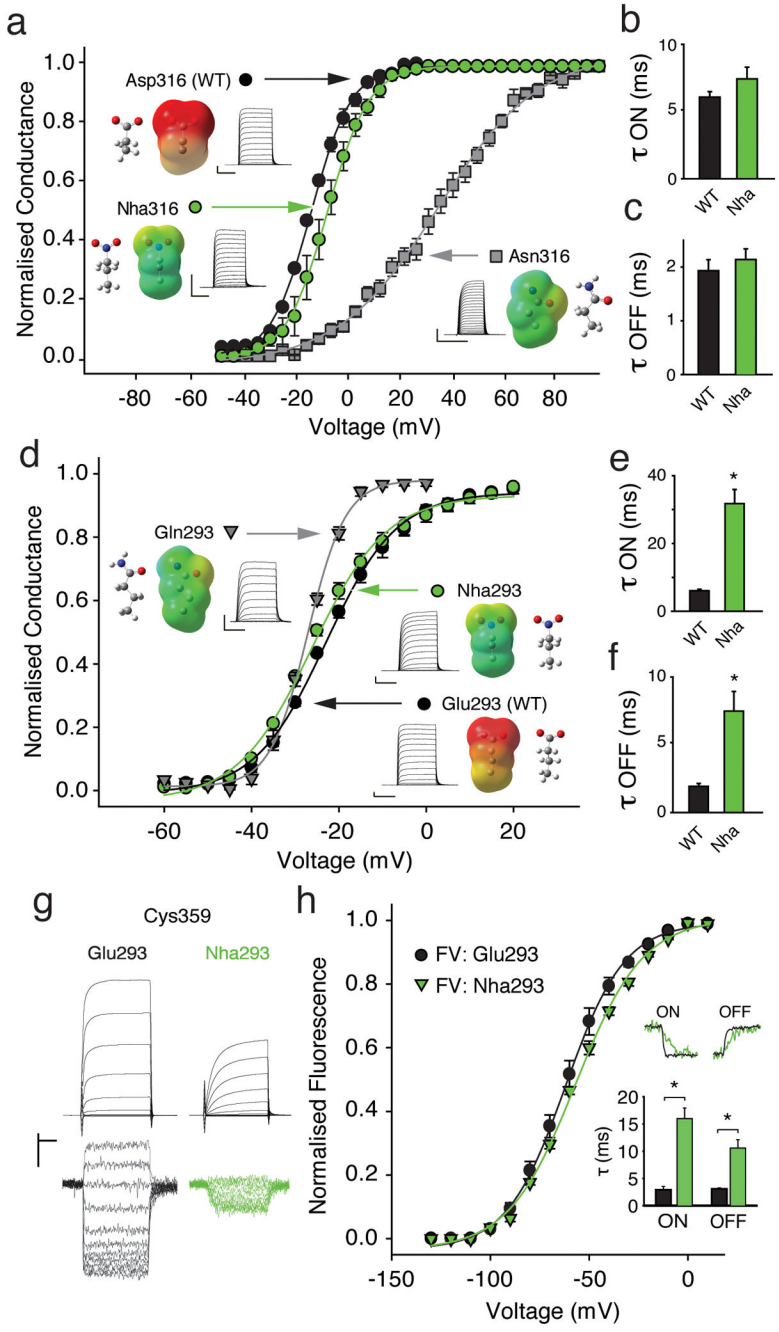

Figure 2. Contributions of Asp 316 and Glu293

(a) GV of natural (Asp, Asn) and unnatural (Nha) side-chains at position 316 (Asn316: $V_{1/2}$ = 27.8 ± 3.3 mV; Nha316: $V_{1/2}$ = −17.5 ± 2.3 mV; Asp316 (WT): $V_{1/2}$ = −22.1 ± 0.7 mV, (n = 5–6)); insets show currents, electrostatic surface potential (ESP, red = −100 kcal/mol, green = 0 kcal/mol, blue = +100 kcal/mol) maps and energy minimized structures of side-chains; (b)/(c) Activation time constants (−80 mV to −25 mV) and deactivation time constants (+20 mV to −25 mV) for Asp316 and Nha316 (single exponential fit, n = 5); (d) GV of natural (Glu, Gln) and unnatural (Nha) side-chains at position 293; insets as in (a); (Gln293: $V_{1/2}$ = −27.1 ± 0.5 mV; Nha293: $V_{1/2}$ = −24.8 ± 0.8 mV; Glu293 (WT): $V_{1/2}$ =

−22.1 ± 0.7 mV (n = 4–6)); (e)/(f) Time constants of activation (e) and deactivation (f) for Glu293 and Nha293 (n = 5–7); protocol as in (b)/(c)); (g) Current (upper panel) and fluorescence (lower panel) recordings for Glu293 (WT) or Nha293 background, in black and green, respectively; (h) FV for Glu293 and Nha293 ($V_{1/2}$: −63.1 ± 3.0 mV and 58.3 ± 1.8 mV, respectively; n = 4). Upper inset shows fluorescence sample traces (ON: −80 mV to −50 mV, OFF: +20 mV to −50 mV); lower inset shows averaged time constants (n = 4). Scale bars: 2 μA for current, 1 % for fluorescence and 50 ms for time (except 20 ms for Asn316). Asterisk indicates significant difference ($p < 0.05$).

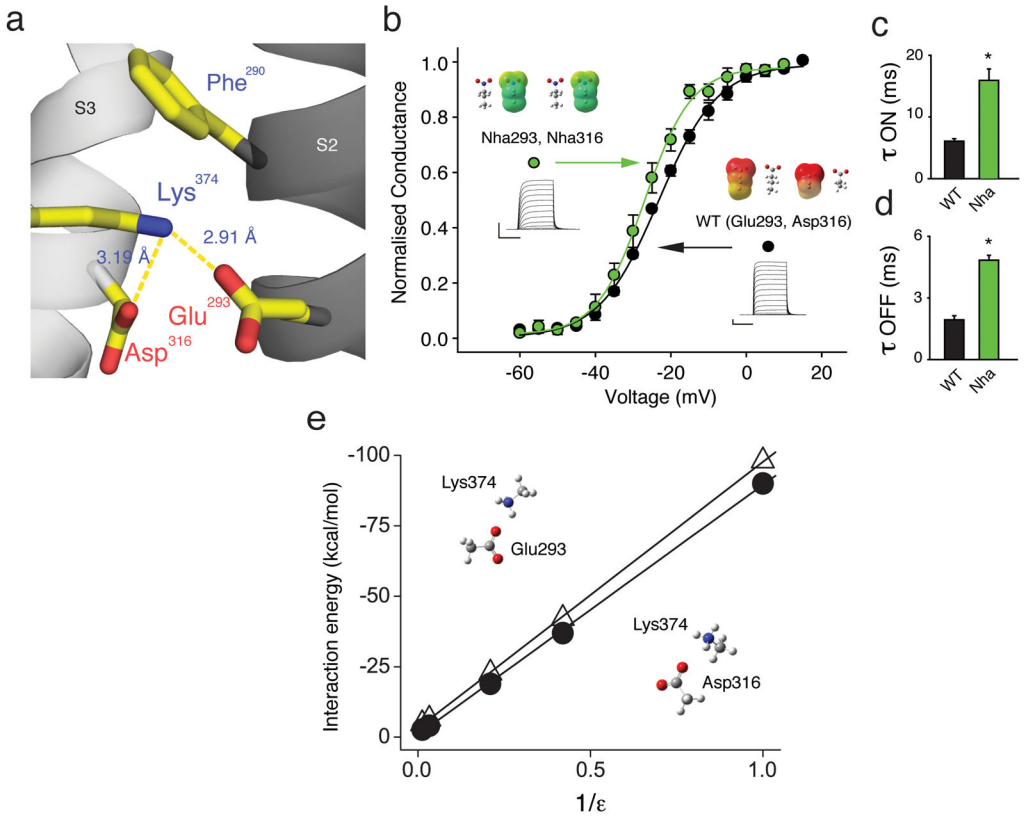

Figure 3. Glu293 and Asp316 do not contribute to a network of electrostatic charge-charge interactions

(a) Model highlighting the proximity of Glu293 and Asp316 to Lys374 (PDB 2R9R); (b) Incorporating Nha simultaneously at positions 293 and 316 has only a minor effect on the GV ($V_{1/2}$ = −27.2 ± 0.9 mV for Nha at positions 293 and 316 vs. $V_{1/2}$ = −22.1 ± 0.7 mV for Glu in position 293 and Asp in position 316 (WT), n = 5); insets show currents, ESP maps and energy minimized structures with scale as in Fig. 2a; (c)/(d) Time constants of activation obtained from a depolarizing pulse from −80 mV to −25 mV (c) and time constants of deactivation obtained from a repolarizing pulse from +20 mV to −25 mV (d) for WT and for Nha simultaneously at positions 293 and 316 (all data fit with a single exponential, n = 5); asterisk indicates significant difference ($p < 0.05$); (e) Plot shows *ab initio* interaction energies at the HF/6-31G*+ level between Lys374 and Glu293 or Asp316 (open triangles or filled circles, respectively) in different dielectric environments. Side-chain moieties from PDB 2R9R were isolated, fixed and modeled as acetate (Glu and Asp) and methylammonium (Lys) in a variety of dielectric environments. All scale bars: 2 μA for current and 50 ms for time.

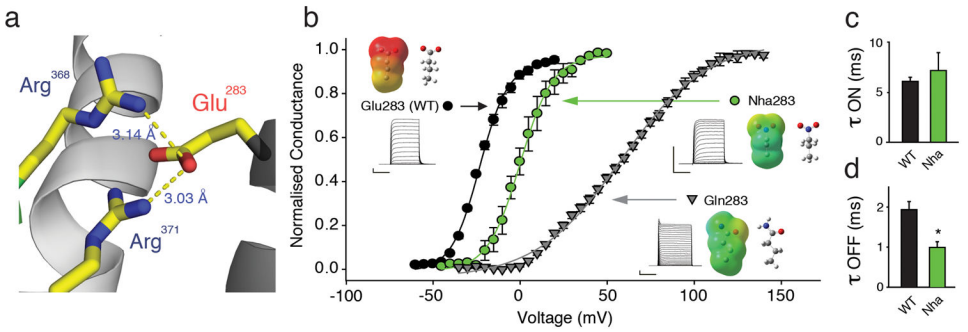

Figure 4. Glu283 is likely to form a state-dependent electrostatic charge-charge interaction with S4 charges

(a) Model highlighting the proximity of Glu283 to Arg 368 and Arg371 (PDB 2R9R); (b) Effects on GV by natural (Glu, Gln) and unnatural (Nha) side-chains at position 283 ($V_{1/2}$ = 58.1 ± 2.0 mV for Gln283 (n = 4); $V_{1/2}$ = 0.9 ± 2.1 mV for Nha283 (n = 8) and $V_{1/2}$ = −22.1 ± 0.7 mV for Glu283 (WT)); insets show currents, ESP maps and energy minimized structures of natural and unnatural amino acids used at position 283 with scale for ESPs as in Fig. 2a; (c)/(d) Time constants of activation obtained from a depolarizing pulse from −80 mV to −25 mV (c) and time constants of deactivation obtained from a repolarizing pulse from from +20 mV (WT) or +40 mV (Nha283) to −25 mV (d) with Nha at positions 293 and 316 (all data fit with a single exponential, n = 5); asterisk indicates significant difference ($p < 0.05$); Scale bars: 2 μA for current, 50 ms for time.

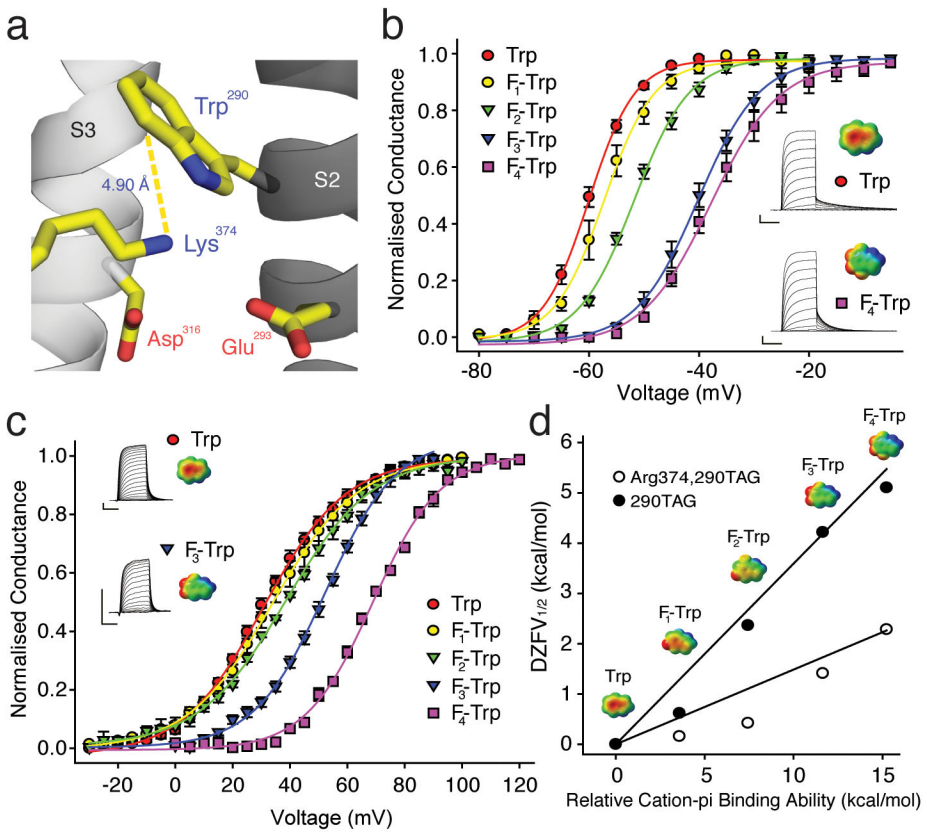

Figure 5. A cation-pi interaction in the potassium channel voltage-sensor

(a) A model highlighting the proximity of Trp290 and Lys374 (PDB 3LNM); (b) Effect of fluorination at Trp290 on GV; insets show currents and ESPs for Trp (upper) and 4,5,6,7-F_4-Trp (lower) (n = 5–7); scale for ESPs: red = −25 kcal/mol, green = 0 kcal/mol, blue = +25 kcal/mol; Scale bars: 2 μA for current, 50 ms for time; (c) Effect of fluorination at Trp290 on the Arg374 background; insets show currents and ESPs for Trp (upper) and 5,6,7-F_4-Trp (lower) (n = 4–6); scale for ESPs as in (b); (d) Cation-pi plot for fluorination of Trp290 with Lys or Arg in position 374. ESPs for Trp derivatives are shown with scales as in (b).